Experimental Wavelet Analysis of Flexural Waves in Beams

by H. Inoue, K. Kishimoto and T. Shibuya

ABSTRACT—The wavelet transform (WT) is applied to the time-frequency analysis of flexural waves in beams. The WT with the Gabor wavelet decomposes a dispersive wave into each frequency component in the time domain, which enables one to determine the traveling time of a wave along the beam at each frequency. By utilizing this fact, a method is developed to identify the dispersion relation and impact site of beams.

Introduction

Analysis of wave propagation in structures is a fundamental subject related to a wide range of engineering problems. Since structural waves are often dispersive, identification of the dispersive characters is important for understanding the wave propagation phenomenon. To identify the dispersive characters, the time-frequency analysis may be one of the most sophisticated techniques among others. Since the time-frequency analysis decomposes a signal into time variations of each frequency component,[1,2] it enables us to examine the propagation of dispersive waves at each frequency.

There have been few studies on the time-frequency analysis of dispersive waves in structures. Hodges, Power and Woodhouse[3] applied the short-time Fourier transform (STFT) to the time-frequency analysis of waves in strings, beams and shells. The STFT has a constant time-frequency resolution, which means that a time-frequency window suitable for analyzing low-frequency components is not adequate for high-frequency components and vice versa. Therefore, the STFT is not suited for analyzing waves composed of a wide range of frequency components. Wahl and Bolton[4] proposed an application of the Wigner-Ville distribution (WVD) to the time-frequency analysis of structural waves. Although the WVD is an optimally concentrated time-frequency distribution, it provides interference terms between each pair of signal components. Wahl and Bolton showed that an appropriate smoothing is required to minimize the interference terms.

To overcome these shortcomings of the STFT or WVD, Kishimoto *et al.*[5] proposed an application of the wavelet transform (WT) to the time-frequency analysis of dispersive waves in structures. The WT is a rather new mathematical technique of time-frequency analysis and has been extensively developed during the last decade.[1,2,6,7] A large number of its applications can be found in a variety of fields of science and engineering. The authors conducted a numerical simulation on flexural waves in a simply supported beam and demonstrated that the WT is an effective tool for identifying the dispersive character of structural waves. However, no experimental verification has confirmed this.

In this paper, we apply the WT to experimental analysis of dispersive waves and demonstrate its usefulness. First, the theory of WT and its application to the time-frequency analysis of dispersive waves are briefly explained. Next, as a typical example of dispersive waves, an experimental analysis of flexural waves in a simply supported beam is presented. In addition, by utilizing the information obtained by the WT, a method to identify the group velocity and impact site of beams is developed.

The Wavelet Transform

The continuous wavelet transform of a function $f(t)$ is defined by[6,7]

$$(Wf)(a,b)=\frac{1}{\sqrt{a}}\int_{-\infty}^{\infty} f(t)\,\overline{\psi\left(\frac{t-b}{a}\right)}\,dt \tag{1}$$

where $a > 0$ and the overline indicates the complex conjugate. The function $\psi(t)$ is called the analyzing wavelet. It satisfies the admissibility condition

$$\int_{-\infty}^{\infty}\frac{|\hat{\psi}(\omega)|^2}{|\omega|}\,d\omega<\infty \tag{2}$$

where $\hat{\psi}(\omega)$ denotes the Fourier transform of $\psi(t)$ defined by

$$\hat{\psi}(\omega)=\int_{-\infty}^{\infty}\psi(t)e^{-i\omega t}\,dt \tag{3}$$

Although there are many choices for the analyzing wavelet, we adopt the Gabor wavelet, since it provides the best time frequency resolution as confirmed by the uncertainty principle.[6] The Gabor wavelet is expressed as[8]

$$\psi_g(t)=\frac{1}{\sqrt[4]{\pi}}\frac{\sqrt{\omega_0}}{\gamma}\exp\left[-\frac{(\omega_0/\gamma)^2}{2}t^2\right]\exp(i\omega_0 t) \tag{4}$$

and its Fourier transform is expressed as

H. Inoue (SEM Member) is Associate Professor, K. Kishimoto and T. Shibuya are Professors, Department of Mechanical and Intelligent Systems Engineering, Tokyo Institute of Technology, 2-12-1, O-okayama, Meguro-ku, Tokyo 152, Japan.

Original manuscript submitted: October 17, 1994. Final manuscript received: September 8, 1995.

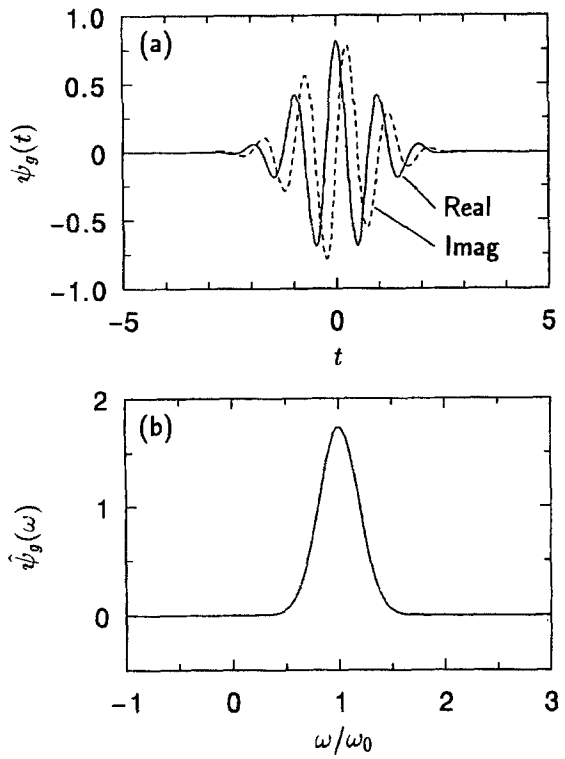

Fig. 1—(a) The Gabor wavelet. (b) The Fourier transform of Gabor wavelet: $\gamma = \pi\sqrt{2/\ln 2}$ and $\omega_0 = 2\pi$

$$\hat{\psi}_g(\omega) = \frac{\sqrt{2\pi}}{\sqrt[4]{\pi}}\sqrt{\frac{\gamma}{\omega_0}}\exp\left[-\frac{(\gamma/\omega_0)^2}{2}(\omega-\omega_0)^2\right] \tag{5}$$

where ω_0 and γ are positive constants. Although the Gabor wavelet does not satisfy the admissibility condition (2) in the strict sense, it approximately satisfies the condition if γ is sufficiently large.[7,9] In this study, we set $\gamma = \pi\sqrt{2/\ln 2} \approx 5.336$ according to Goupillaud, Grossmann and Morlet.[9] If eq (4) is substituted into eq (1), it is understood that the WT using the Gabor wavelet has a similar form to the Fourier transform with Gaussian windowing. Hence we set $\omega_0 = 2\pi$ such that $1/a$ takes the same value as the frequency $\omega/(2\pi)$.

Figure 1 shows the Gabor wavelet and its Fourier transform. The Gabor wavelet $\psi_g(t)$ is localized around the time $(t) = 0$, and its Fourier transform $\hat{\psi}_g(\omega)$ is localized around the angular frequency $\omega = \omega_0$. It is easily understood that the function $\psi_g((t-b)/a)$ is localized around $t = b$ and that its Fourier transform $[a\exp(-ib\omega)\hat{\psi}_g(a\omega)]$ is localized around $\omega = \omega_0/a$. Hence the magnitude of WT, $|(Wf)(a, b)|$, represents the "intensity" of the signal $f(t)$ around the time $t = b$ and the angular frequency $\omega = \omega_0/a$.

Wavelet Analysis of Dispersive Waves

Let us consider two harmonic waves of unit amplitude and different angular frequency ω_1 and ω_2 propagating in the x-direction, given by

$$\begin{aligned} u(x, t) &= e^{-i(k_1 x - \omega_1 t)} + e^{-i(k_2 x - \omega_2 t)} \\ &= 2\cos(\Delta k x - \Delta\omega t)\, e^{-i(k_c x - \omega_c t)} \end{aligned} \tag{6}$$

where k_1 and k_2 are wave numbers,

$$k_c = (k_1 + k_2)/2,\ \omega_c = (\omega_1 + \omega_2)/2 \tag{7}$$

and

$$Dk = (k_1 - k_2)/2,\ \Delta\omega = (\omega_1 - \omega_2)/2 \tag{8}$$

If $\Delta\omega$ is sufficiently small, the group velocity c_g at the angular frequency ω_c can be defined as

$$c_g = \Delta\omega/\Delta k \tag{9}$$

When the Gabor wavelet is adopted as the analyzing wavelet, the magnitude of WT of $u(x, t)$ is obtained as[5]

$$\begin{aligned} &|(Wu)(x, a, b)| = \\ &\sqrt{a}\left\{[\hat{\psi}_g(a\omega_1)]^2 + [\hat{\psi}_g(a\omega_2)]^2\right. \\ &\left. + 2\hat{\psi}_g(a\omega_1)\hat{\psi}_g(a\omega_2)\cos(2\Delta k x - 2\Delta\omega b)\right\}^{1/2} \end{aligned} \tag{10}$$

If $\Delta\omega$ is sufficiently small such that $\hat{\psi}_g(a\omega_1) \simeq \hat{\psi}_g(a\omega_2) \simeq \hat{\psi}_g(a\omega_c)$, we obtain

$$\begin{aligned} &|(Wu)(x, a, b)| \simeq \sqrt{2a}\,\hat{\psi}_g(a\omega_c) \\ &[1 + \cos(2\Delta k x - 2\Delta\omega b)]^{1/2} \end{aligned} \tag{11}$$

This equation indicates that the magnitude of WT takes its maximum value at $a = \omega_0/\omega_c$ and $b = (\Delta k/\Delta\omega)x = x/c_g$. Therefore, for fixed x, a three-dimensional plot of $|(Wu)(x, a, b)|$ on the (a, b) -plane has a peak at $(a, b) = (\omega_0/\omega_c, x/c_g)$. In other words, the location of the peak on the (a, b) -plane indicates the arrival time $b = x/c_g$ of the wave having angular frequency $\omega_c = \omega_0/a$.

Flexural Waves in a Simply Supported Beam

As a typical example of dispersive waves in structures, we conducted an experimental analysis of flexural waves propagating in a simply supported beam.

Experimental Setup

Figure 2 shows the experimental setup. A simply supported beam with circular cross section was impacted with a steel ball (19-mm diameter) at the center of the span (point A). Table 1 shows dimensions and material constants of the beam. Bending strains were measured at points B, C and D by using strain gages as shown in Fig. 2. The onset of impact and the contact duration were also measured by using the DC circuit illustrated in the figure. The

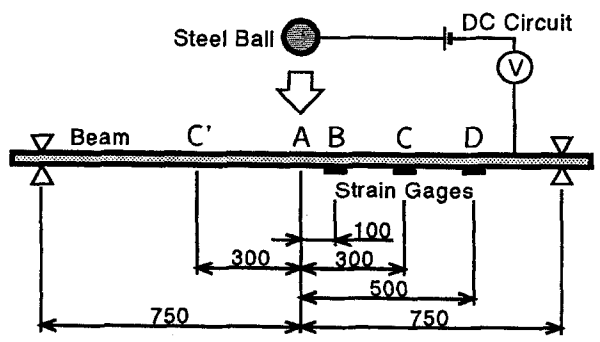

Fig. 2—Simply supported beam subjected to impact at the center of the span (dimensions in mm)

TABLE 1—DIMENSIONS AND MATERIAL CONSTANTS OF THE BEAM

Span	1.5 m
Diameter	20 mm
Cross-sectional area	3.14×10^{-4} m^2
Moment of inertia	7.85×10^{-9} m^4
Timoshenko's shear coefficient (after Mindlin and Deresiewicz[10])	0.847
Young's modulus	98.1 GPa
Mass density	8.65×10^3 kg/m^3

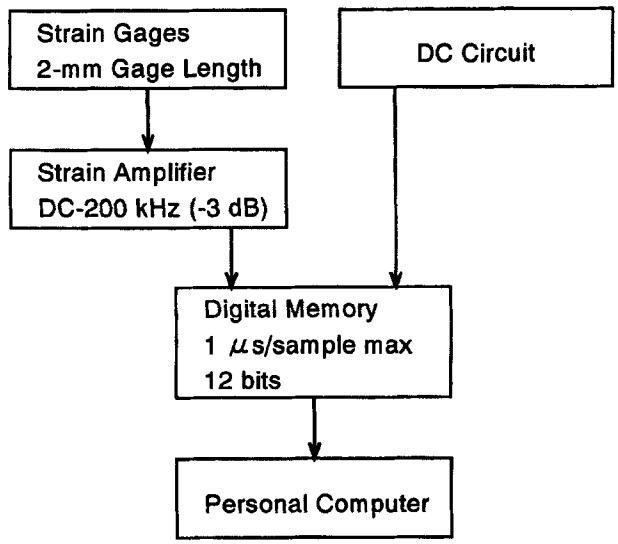

Fig. 3—Measurement system

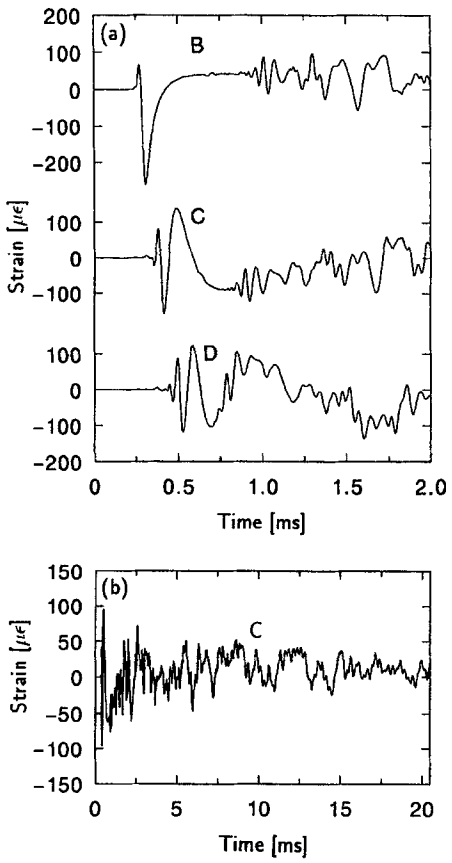

Fig. 4—Bending strains measured at points B, C and D. (a) Δt = 1 μs. (b) Δt = 10 μs

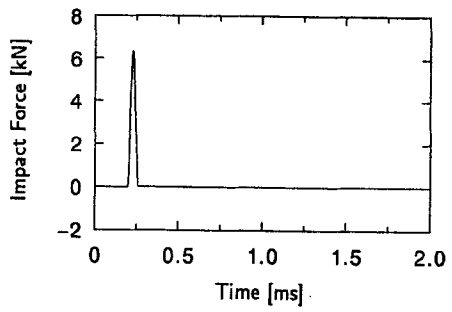

Fig. 5—Impact force history predicted by Schwieger's method

measurement system used is shown in Fig. 3. The data were sampled at the rate Δt = 1 or 10 μs/sample.

Measured Strain

Figure 4(a) shows the strains measured at points B, C and D, where the data were sampled at the rate Δt = 1 μs/sample. The impact velocity was 4.43 m/s, the onset of impact t = 0.2 ms and the contact duration 65 μs. It is seen that the rising of the time history becomes ambiguous as the wave propagates. Figure 4(b) shows the strain measured at point C in the case Δt = 10 μs/sample. Figure 5 shows the impact force history predicted by Schwieger's method,[11] in which Hertzian contact between the sphere and cylinder[12] is assumed. The predicted contact duration is 60 μs, which agrees fairly well with the measured duration of 65 μs.

Wavelet Transformation

The WTs of the strains and the impact force were computed according to eq (1). The integral in eq (1) was evaluated by truncating the limit of integration from $t = b - 4a$ to $t = b + 4a$ and by applying the trapezoidal rule with a step equal to the sampling rate Δt. The parameters a and b were discretized as follows:

$$a = 2^{m/4}, \quad b = n\Delta t \tag{12}$$

where m and n are integers. The discretization of the parameter a seems unusual but is common in most applications of the WT. On the other hand, the parameter b is usually discretized as $b = an\Delta t$. The reason why the parameter b is discretized as in eq (12) is that we require a good time resolution to identify the group velocity and impact site by the method described below.

Figure 6(a) shows the magnitude of WT of the impact force, and Figs. 6(b)-(d) show those of the strains at points B, C and D, respectively. In these figures, the WT is plotted at every 10 points of actual data in the b-axis. In Fig. 6(a), a "ridge" appears around b = 0.2 ms in the low-frequency range, $\log_2 a \geq -15$ ($\omega_0/(2\pi a) \leq 33$ kHz), and it divides into two in the high-frequency range, $\log_2 a \leq -15$ ($\omega_0/(2\pi a) \geq 33$ kHz). This indicates that the rising and ending of the force history are no longer distinguished in the low-frequency

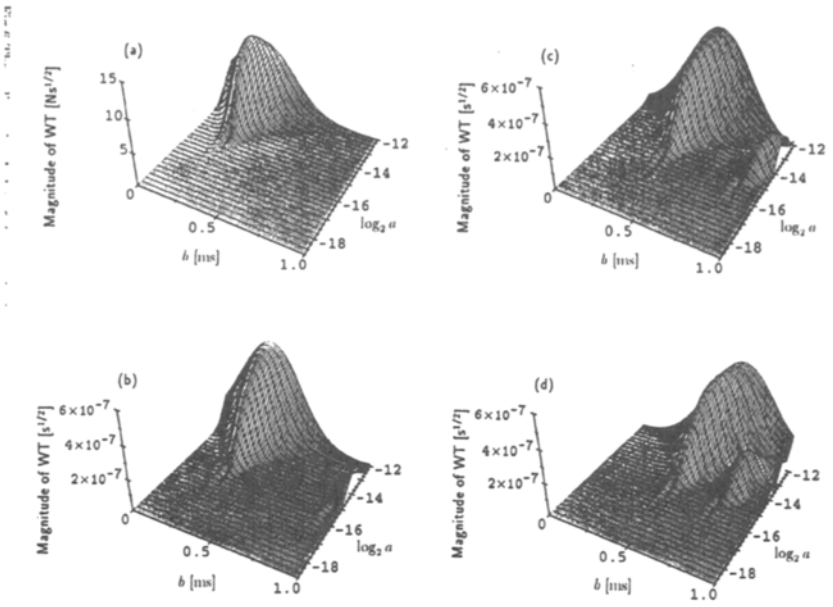

Fig. 6—Three-dimensional plot of the magnitude of WT. (a) Impact force history. (b)-(d) Strains at points B, C and D, Δt = 1 μs

range because the width of the time window is larger than the contact duration. In Figs. 6(b)-(d), two ridges can be found. The larger ridge appearing around b = 0.3 ms in Fig. 6(b) corresponds to that found in Fig. 6(a) and moves toward the positive b-direction as the measuring point approaches the support [see Figs. 6(c)-(d)]. Therefore, the larger ridge represents the wave traveling outward from the impact site. On the other hand, the smaller ridge appearing around b = 1.0 ms in Fig. 6(b) moves toward the negative b-direction [see Figs. 6(c)-(d)], representing the wave reflected at the support.

Figure 7 shows the magnitude of WT of the strain at point C for a wider range of time, where Δt = 10 μs/sample. In the figure, the WT is plotted at every five points of actual data in the b-axis. The ridges found in Fig. 6(c) also appear in this figure but are obscured in the low-frequency range. This may be due to the stationary vibration of the beam.[5]

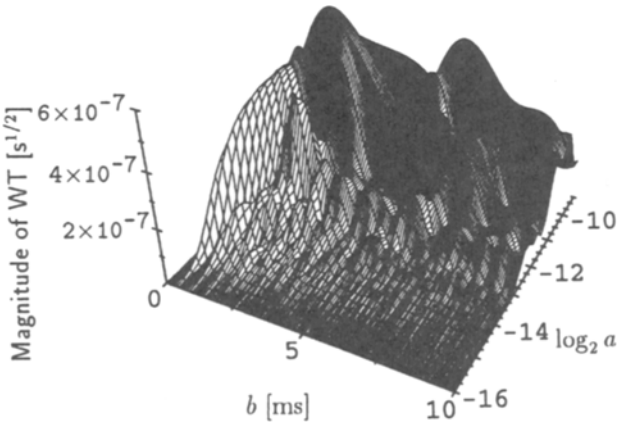

Fig. 7—Three-dimensional plot of the magnitude of WT of the strain at point C, Δt = 10 μs

Arrival Time

As mentioned above, the magnitude of WT takes its maximum value at the time b when the wave arrives at the measuring point for each value of a. We numerically extracted the positions where the WT takes its maximum value on the (a, b) -plane for each value of a. The result is plotted in Fig. 8. The curves shown in Fig. 8 indicate the arrival times predicted by the Pochhammer-Chree theory,[13,14] where it is assumed that all frequency components were initiated from the impact site at the onset of impact, t = 0.2 ms, and directly arrived at each measuring point.

In the range of $-16.25 \le \log_2 a \le -15.25$ (78 kHz $\ge \omega_0/(2\pi a) \ge$ 39 kHz), the arrival times obtained by the wavelet analysis coincide well with those predicted by the theory. In the range of $-15 \le \log_2 a \le -11$ (33 kHz $\ge \omega_0/(2\pi a) \ge$ 2 kHz), there is a time lag about 33 μs, which is comparable to a half of the contact duration. As mentioned above, this is due to the fact that the width of the time window becomes larger than the contact duration in this low-frequency range. However, it should be noted that the amount of this time lag is constant for all measuring points. In much lower frequency range, $\log_2 a \ge -11$ ($\omega_0/(2\pi a) \le$ 2 kHz), the arrival time cannot be extracted, since the transient response is obscured by the stationary vibration of the beam. In the higher frequency range, $\log_2 a \le -16.5$ ($\omega_0/(2\pi a) \ge$ 93 kHz), the arrival time could not be extracted accurately because of the poor signal-to-noise ratio of the data due to limitations of the measuring equipment.

Identification of the Group Velocity and Impact Site

There have been some methods for experimentally identifying the velocity of structural waves as a function of fre-

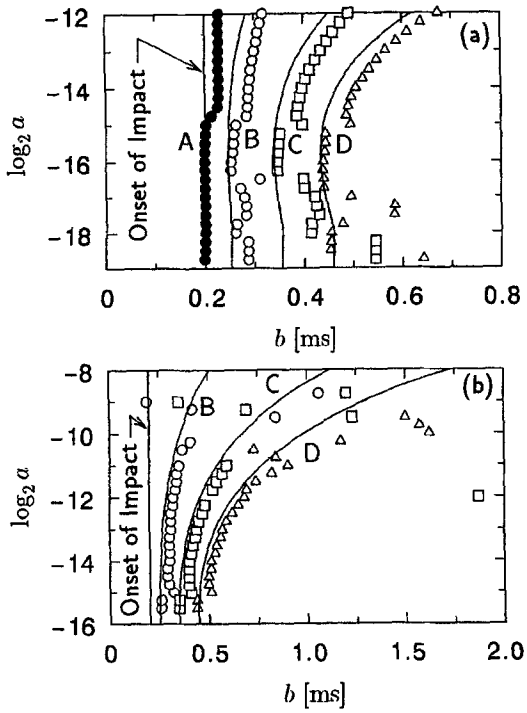

Fig. 8—Arrival time of each frequency component of the flexural wave at points B, C and D. (a) Δt = 1 μs. (b) Δt = 10 μs

quency. A common technique is the resonance method, in which the phase velocity is determined from the measurement of resonant frequencies of structures.[15,16] However, it requires repetitious measurements at various frequencies to obtain the frequency dependence of the wave velocity.

Estimation of the impact site of structures has been tackled by several researchers. Doyle[17] has proposed a method to estimate the impact site of beams by utilizing the phase information obtained by using the Fourier transform. However, the use of the phase information requires the computation of $\tan^{-1}$, which may be rather troublesome.

As shown above, the wavelet analysis of dispersive waves provides the arrival time of each frequency component. By utilizing this fact, we can identify the group velocity at each frequency and, in addition, estimate the impact site.

Let us consider two points P_1 and P_2 on one side and a point P_3 on the other side of the impact site P_0 as shown in Fig. 9. The distances of these points from the impact site are denoted by l_1, l_2 and l_3, respectively. Suppose that the arrival time of the wave at the point P_k is extracted by the wavelet analysis and is denoted by $b_k(a)$. Note that the time origin is arbitrary. In addition, let us consider the unknown time lag $b_0(a)$, which arises when the width of the time window becomes larger than the contact duration. Then we obtain

$$b_k(a) = b_0(a) + l_k/c_g(a), \ (k = 1, 2, 3) \qquad (13)$$

where $c_g(a)$ is the group velocity.

Subtracting $b_1(a)$ from $b_2(a)$, we obtain

$$c_g(a) = \frac{l_2 - l_1}{b_2(a) - b_1(a)} \qquad (14)$$

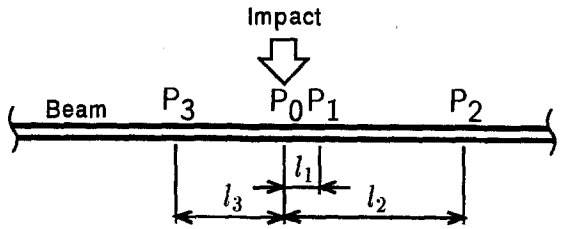

Fig. 9—Identification of group velocity and estimation of impact site

On the other hand, adding $b_1(a)$ to $b_3(a)$, we obtain

$$b_0(a) = \frac{1}{2}\left[b_1(a) + b_3(a) - \frac{l_1 + l_3}{c_g(a)}\right] \qquad (15)$$

Since $b_1(a)$, $b_2(a)$ and $b_3(a)$ are obtained by the wavelet analysis of experimental data and, in addition, $(l_2 - l_1)$ and $(l_1 + l_3)$ are known in advance, the group velocity $c_g(a)$ and the time lag $b_0(a)$ can be identified for each value of a, namely, for each frequency. Once $c_g(a)$ and $b_0(a)$ are identified, the distances l_1, l_2 and l_3 can be easily determined by eq (13).

We considered the points A, B and D in this experiment as the points P_0, P_1 and P_2, respectively, and identified the group velocity for each value of a from the arrival times shown in Fig. 8(a). Figure 10 shows the results, in which the curves are predictions by the Bernoulli-Euler, Timoshenko and Pochhammer-Chree theories. The identified velocity agrees well with the prediction by the exact Pochhammer-Chree theory for a very wide range of frequency 4 kHz $\leq \omega_0/(2\pi a) \leq$ 78 kHz ($-12 \geq \log_2 a \geq -16.25$). The scatter in the high-frequency range is due to the errors mentioned above.

Since the impact response of the beam is symmetric about the impact site in this experiment, the strain at point C′ in Fig. 2 is same as that at point C. Therefore, we considered the strain at point C as that at point P_3 and estimated the time lag $b_0(a)$ and the distance l_1. The estimated distance l_1 is shown in Fig. 11. The impact site is accurately estimated except for the high-frequency range.

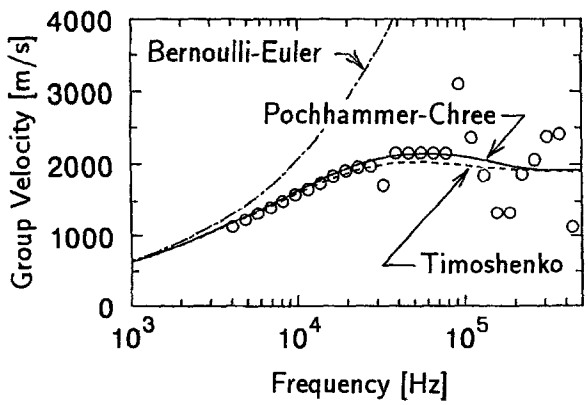

Fig. 10—Group velocity identified by the wavelet analysis

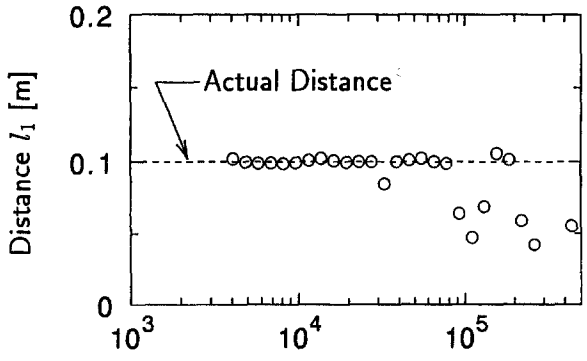

Fig. 11—Impact site estimated by the wavelet analysis

Conclusions

In this study, an application of the wavelet transform (WT) to the experimental time-frequency analysis of dispersive waves in structures has been presented. It has been shown that the WT using the Gabor wavelet is an effective tool for the experimental analysis of dispersive waves. The three-dimensional plot of the magnitude of WT on the time- frequency plane has peaks whose locations indicate the arrival times of each frequency component of the wave. In addition, a method has been developed to identify the group velocity and impact site of beams by utilizing the arrival times extracted by the wavelet analysis.

Although the example treated in this study is rather classical, the time-frequency analysis of elastic waves by means of the WT will be applicable to various problems in experimental mechanics, such as the material evaluation by ultrasonics and the source identification of acoustic emissions.

Acknowledgment

The authors appreciate Tomoaki Nakanishi, graduate student at the Tokyo Institute of Technology, for his assistance in this experiment and data processing.

References

1. *Rioul, O. and Vetterli, M., "Wavelets and Signal Processing," IEEE Signal Processing Magazine,* **8** *(4), 14–38 (1991).*

2. *Hlawatsch, F. and Boudreaux-Bartels, G.F., "Linear and Quadratic Time-frequency Signal Representations," IEEE Signal Processing Magazine,* **9** *(2), 21–67 (1992).*

3. *Hodges, C.H., Power, J. and Woodhouse, J., "The Use of the Sonogram in Structural Acoustics and an Application to the Vibrations of Cylindrical Shells," J. Sound Vib.,* **101** *(2), 203–218 (1985).*

4. *Wahl, T.J. and Bolton, J.S., "The Application of the Wigner Distribution to the Identification of Structure-Borne Noise Components," J. Sound Vib.,* **163** *(1), 101–122 (1993).*

5. *Kishimoto, K., Inoue, H., Hamada, M. and Shibuya, T., "Time-frequency Analysis of Dispersive Waves by Means of Wavelet Transform," Trans. ASME, J. Appl. Mech.* **62** *(4), 841-846 (1995).*

6. *Chui, C.K., An Introduction to Wavelets, Academic Press, San Diego (1992).*

7. *Daubechies, I., Ten Lectures on Wavelets, SIAM, Philadelphia (1992).*

8. *Sato, M., "Mathematical Foundation of Wavelets," J. Acoust. Soc. Japan,* **47** *(6), 405–423 (1991) (in Japanese).*

9. *Goupillaud, P., Grossmann, G. and Morlet, J., "Cycle-Octave and Related Transforms in Seismic Signal Analysis," Geoexploration,* **23**, *85–102 (1984).*

10. *Mindlin, R.D. and Deresiewicz, H., "Timoshenko's Shear Coefficient for Flexural Vibrations of Beams," Proc. Second U.S. Nat. Cong. of Appl. Mech., ASME, 175–178 (1954).*

11. *Schwieger, H., "A Simple Calculation of the Transverse Impact on Beams and Its Experimental Verification,"* EXPERIMENTAL MECHANICS, **5** *(11), 378–384 (1965).*

12. *Johnson, K.L., Contact Mechanics, Cambridge University Press, Cambridge (1985).*

13. *Graff, K.F., Wave Motion in Elastic Solids, Reprint Ed., Dover Publications, New York (1991).*

14. *Pao, Y.H. and Mindlin, R.D., "Dispersion of Flexural Waves in an Elastic, Circular Cylinder," Trans. ASME, J. Appl. Mech.,* **27**, *513–520 (1960).*

15. *Zemanik, J. and Rudnick, I., "Attenuation of Dispersion of Elastic Waves in a Cylindrical Bar," J. Acoust. Soc. Am.,* **33** *(10), 1283–1288 (1961).*

16. *Kolsky, H., Stress Waves in Solids, Reprint Ed., Dover Publications, New York (1963).*

17. *Doyle, J.F., "An Experimental Method for Determining the Location and Time of Initiation of an Unknown Dispersive Pulse,"* EXPERIMENTAL MECHANICS, **27** *(3), 229–233 (1987).*